ACS APPLIED MATERIALS & INTERFACES

Research Article

www.acsami.org

Self-Supported Single Crystalline $H_2Ti_8O_{17}$ Nanoarrays as Integrated Three-Dimensional Anodes for Lithium-Ion Microbatteries

Jin-Yun Liao,[†] Xingcheng Xiao,*[,‡] Drew Higgins,[†] Gregory Lui,[†] and Zhongwei Chen*[,†]

[†]Department of Chemical Engineering, Waterloo Institute for Nanotechnology, University of Waterloo, 200 University Avenue West, Waterloo, Ontario, Canada N2L 3G1

[‡]General Motors Global Research & Development Center, 30500 Mound Road, Warren, Michigan 48090, United States

Supporting Information

ABSTRACT: Well-ordered, one-dimensional $H_2Ti_2O_5$, $H_2Ti_8O_{17}$, TiO_2−B, and anatase TiO_2/TiO_2−B nanowire arrays were innovatively designed and directly grown on current collectors as high performance three dimensional (3D) anodes for binder and carbon free lithium ion batteries (LIBs). The prepared thin nanowires exhibited a single crystalline phase with highly uniform morphologies, diameters ranging from 70−80 nm, and lengths of around 15 μm. Specifically, reversible Li insertion and extraction reactions around 1.6−1.8 V with initial intercalation capacities of 326 and 271 mA h g^{-1} at a cycling rate of 0.1 C (where 1 C = 335 mA g^{-1}) were observed for $H_2Ti_8O_{17}$ and TiO_2−B nanowire arrays, respectively. Among the four compounds investigated, the $H_2Ti_8O_{17}$ nanowire electrode demonstrated optimal cycling stability, delivering a high specific discharge capacity of 157.8 mA h g^{-1} with a coulombic efficiency of 100%, even after the 500th cycle at a current rate of 1 C. Furthermore, the $H_2Ti_8O_{17}$ nanowire electrode displayed superior rate performance with rechargeable discharge capacities of 127.2, 111.4, 87.2, and 73.5 mA h g^{-1} at 5 C, 10 C, 20 C, and 30 C, respectively. These results present the potential opportunity for the development of high-performance LIBs based on nanostructured Ti-based anode materials in terms of high stability and high rate capability.

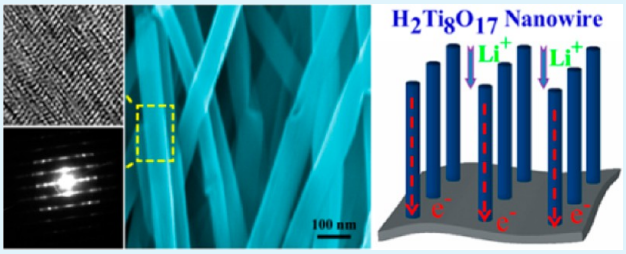

KEYWORDS: *$H_2Ti_8O_{17}$, Li-ion batteries, nanowire, 3D, microbatteries*

1. INTRODUCTION

Lithium-ion batteries (LIBs) with prominent advantages of high energy and power density as well as long cycling life have now shown that they have a promising future in the coming era of hybrid electric vehicles (HEVs) and electric vehicles (EVs).[1−7] However, the commercialization of LIB based electric vehicles has proceeded slower than projected. This is partially due to two pertinent technical challenges facing the commercial carbon based anode materials (typically graphite), particularly, (i) that unstable SEI formed on graphite below 1 V might lead to low columbic efficiency and (ii) safety concerns arising due to lithium dendrite formation which occurs because of the Li-intercalation potential of graphite approaching 0 V (vs Li/Li^+).[8−11] Furthermore, at high charge−discharge rates, the slow Li^+ diffusion in the graphite anode materials will be a significant source of polarization, resulting in decreased power density and effectively limiting the practical application in commercial HEVs/EVs.[12−15]

Being inherently safe and chemically compatible with the electrolyte, titanium (Ti) based materials (anatase TiO_2, TiO_2−B, $Li_4Ti_5O_{12}$) with high operating voltages (>1 V vs Li/Li^+) that ensure improved safety are considered the most promising alternatives to the conventional anode materials used in LIBs.[16−20] Furthermore, the negligible structural and volumetric changes occurring during Li ion insertion/extraction can lead to excellent overall cycling stability.[8,21,22] Among the Ti-based compounds investigated, TiO_2−B has emerged as a promising candidate boasting a high theoretical capacity of 335 mA h g^{-1}.[23] On other hand, Idemoto et al. recently reported the use of $H_2Ti_{12}O_{25}$ as novel anode materials for LIBs and depicted a higher capacity of 225 mA h g^{-1} compared to $Li_4Ti_5O_{12}$ (175 mA h g^{-1}) with excellent cycling performance.[24] This successfully illustrated the promise of using hydrogen titanium oxides (HTO) as a new class of anode materials for LIB applications.[8,25,26]

Despite the inherent safety and cyclability advantages, the rate capabilities of Ti-based anode materials are relatively low due to the poor electrical conductivity and sluggish Li-ion diffusion kinetics, inevitably resulting in a large polarization at high charge/discharge rates.[8] In order to overcome these drawbacks, many approaches have been reported to improve the battery performance, such as carbon coating, metal/non-metal ion doping, etc.[18,27,28] Furthermore, most of these anode materials need to be mixed with carbon black and a binder and then pressed onto an electrode substrate prior to battery assembly. Apart from the development of advanced anode

Received: October 21, 2013
Accepted: December 13, 2013
Published: December 13, 2013

materials to meet traditional application needs, new electrode designs are being extensively investigated for their potential to meet the power demands of micro-electronics, a rapidly emerging field. These advanced micro- or nanobaterry designs incorporating unique three-dimensional electrode materials and nanostructure engineering could effectively provide improved electrochemical performance, compared to their planar counterparts for on-board microelectronic applications.[29−31] Recently, self-supported oxide nanowire/tube arrays ($Li_4Ti_5O_{12}$, Co_3O_4, SnO_2, anatase TiO_2) grown directly on current-collecting substrates as 3D anode electrodes have been reported capable of demonstrating high density and fast charge/discharge properties in the absence of electrode additives (i.e., conductive carbon black and binder).[32−35] However, most of the reported one-dimensional (1D) nanostructured LIB anode materials have been limited to polycrystalline structures due primarily to the limitations of existing synthetic techniques. Unfortunately, the performance of 1D polycrystalline nanostructures may be limited due to electron scattering or trapping at grain boundaries, whereas single crystalline 1D nanostructures can offer the potential of direct electrical pathways to increase the electron transport rate and, in turn, improve the LIB performance.[36−38] Therefore, it is highly desirable to fabricate novel single crystalline 1D Ti-based nanowire arrays in direct contact with the electrode current collectors in order to provide enhanced electronic conductivity and further improve the rate capability of LIBs.

In the present work, we have successfully synthesized single crystalline $H_2Ti_2O_5$, $H_2Ti_8O_{17}$, TiO_2−B, and anatase TiO_2/TiO_2−B nanowire arrays directly on a flexible Ti foil. Prepared by subjecting $H_2Ti_2O_5{\cdot}H_2O$ to heat treatment at different temperatures, these nanowires have average diameters of 74 nm and lengths of around 15 μm. For the first time, the electrochemical Li ion insertion/extraction properties of these 3D single crystalline HTO and titanium oxide nanowire array anodes have been characterized, providing a gauge of their practical applicability towards LIBs. The prepared $H_2Ti_8O_{17}$ nanowire based electrode demonstrated optimal performance through direct testing as an anode in a half cell LIB, providing high charge/discharge capacities, excellent rate capabilities, and exemplary cycling performance.

2. EXPERIMENTAL SECTION

Preparation of Electrode. A piece of titanium foil (2.5×2.5 cm^2) ultrasonically cleaned in water, acetone, and ethanol for 15 min each was placed against the wall of a 40 mL Teflon-lined stainless steel autoclave filled with 30 mL of 1 M NaOH aqueous solution. Then, the sealed autoclave was put in an electric oven at 220 °C for 24 h.[39,40] After completion of the hydrothermal reaction, the titanium foil covered with $Na_2Ti_2O_5{\cdot}H_2O$ nanowires was immersed in 0.5 M HCl solution for 2 h to replace Na^+ with H^+, rendering $H_2Ti_2O_5{\cdot}H_2O$ nanowire arrays on Ti foil. Then, the Ti foil was removed from HCl solution and rinsed with water and ethanol and dried at 60 °C for 1 day. Upon heating the as-prepared $H_2Ti_2O_5{\cdot}H_2O$ sample at different temperatures in air, we were able to control the formation of the $H_2Ti_2O_5$, $H_2Ti_8O_{17}$, TiO_2−B, or anatase TiO_2/TiO_2−B phases. The $H_2Ti_2O_5$ sample was prepared by heating as-prepared $H_2Ti_2O_5{\cdot}H_2O$ nanowire arrays on Ti foil at 100 °C in a vacuum oven overnight, whereas the $H_2Ti_8O_{17}$, TiO_2−B, and anatase TiO_2/TiO_2−B samples were prepared at 250 °C, 400 °C, and 550 °C for 2 h in a quartz tube furnace, respectively.

Materials Characterization. The phase purity and crystal structure of the obtained materials were studied using an X-ray diffraction (XRD, Bruker AXS D8 Advance) system with Cu Kα radiation from 5 to 70°. A field emission scanning electron microscope (FE-SEM, LEO FESEM 1530), transmission electron microscope (TEM, Philips CM300), and high-resolution transmission electron microscope (HRTEM) were used to examine the morphologies and crystalline structures of the samples. The FTIR spectra were measured at room temperature by the KBr method using an Avatar 320 FT-IR spectrometer. Thermogravimetric analysis (TGA) was performed using a TGA Q500 V20.10 instrument. The experiment was performed by heating the as-prepared sample (~10 mg) from room temperature to 600 °C at 5 °C min^{-1} in air.

Evaluation of Electrochemical Behavior. The electrochemical characterization was performed using 2032-type coin cells with two electrodes and assembled in an Ar-filled dry glove box using Ti-based nanowire arrays/Ti-foil and Li metal as the working electrode and counter electrode, respectively. The electrolyte was 1 M LiPF6 in ethyl carbonate (EC)/dimethyl carbonate (DMC) (3/7 by volume), and two pieces of porous 25 μm thick polypropylene were used as separators. The discharge−charge cycling was performed between 1.0 and 2.5 V (vs Li/Li^+) at room temperature, using different C-rates on a battery tester (Neware) (1 C = 335 mA g^{-1}). Electrochemical impedance spectroscopy (EIS) was carried out in the frequency range from 100 kHz to 100 mHz on an electrochemical workstation (VersaSTAT MC, Princeton Applied Research), and the amplitude of the alternating voltage was 10 mV. The impedance parameters were determined by fitting of the impedance spectra using Z-view software. To determine the mass of the active materials, the mass and length of the $H_2Ti_2O_5$ nanowires on both sides of the Ti foil was assumed identical. The foils were weighed initially and again after removing the nanowires from one side, with the resultant change used as the active mass. The average active material loading for each electrode is around 1 mg.[31]

3. RESULTS AND DISCUSSION

Upon heating the as-prepared $H_2Ti_2O_5{\cdot}H_2O$ samples, the formation of single phase $H_2Ti_2O_5$, $H_2Ti_8O_{17}$, TiO_2−B, and composite TiO_2/TiO_2−B were obtained at annealing temperatures of 100, 250, 400, and 550 °C for 2 h in air, respectively. The corresponding XRD patterns are shown in Figure 1.

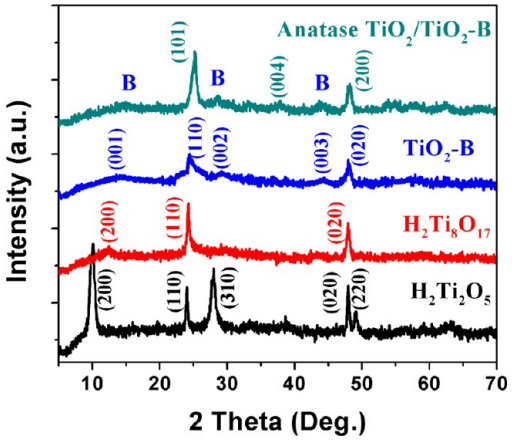

Figure 1. XRD patterns of $H_2Ti_2O_5$, $H_2Ti_8O_{17}$, TiO_2−B, and anatase TiO_2/TiO_2−B prepared at different temperatures.

Specifically, the obtained $H_2Ti_2O_5$ and $H_2Ti_8O_{17}$ samples were identified to be single phase in the XRD patterns, in which the diffraction peaks are well indexed to $H_2Ti_2O_5$ (JCPDS No. 47-0124) and $H_2Ti_8O_{17}$ (JCPDS 36-0656).[17,41] On the other hand, the diffraction peaks in the prepared TiO_2−B XRD pattern can be indexed to the monoclinic TiO_2−B phase (JCPDS No. 74-1940), indicating the successful formation of the TiO_2−B phase at 400 °C. The diffraction peaks at 25.3°, 37.7°, and 48.3° present in the sample treated in air at 550 °C correspond to the

dx.doi.org/10.1021/am4046487 | ACS Appl. Mater. Interfaces 2014, 6, 568−574

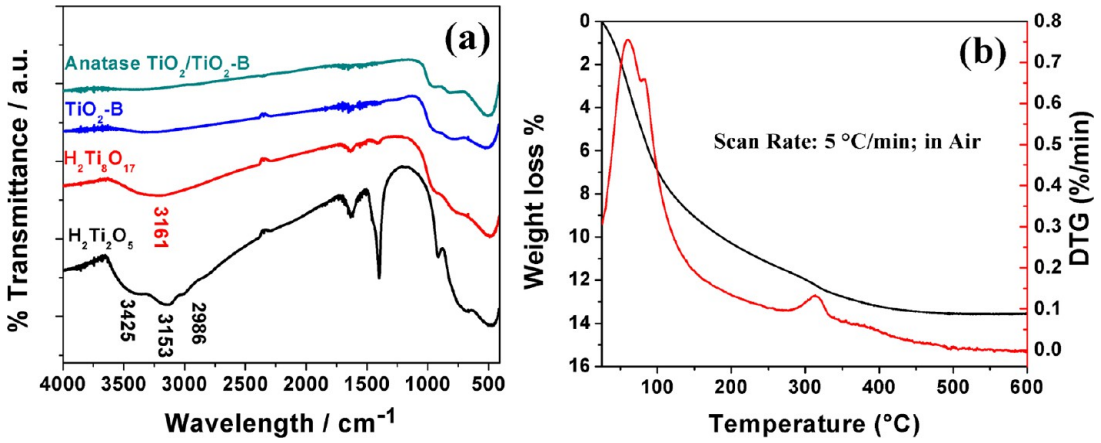

Figure 2. (a) FTIR spectra of $H_2Ti_2O_5$, $H_2Ti_8O_{17}$, TiO_2–B, and anatase TiO_2/TiO_2–B samples; (b) TG and DTG curves of as prepared $H_2Ti_2O_5 \cdot H_2O$ nanowires detached from the Ti substrates.

(101), (004), and (200) lattice planes of anatase (JCPDS No. 65-2900), respectively. These peaks, present along with the characteristic TiO_2–B peaks, indicate the successful coexistence of both of these phases.

Generally, the FTIR spectrum is used to investigate the presence of water species such as H_2O, OH^-, and H_3O^+ in the structures. Figure 2a presents the FTIR spectra of $H_2Ti_2O_5$, $H_2Ti_8O_{17}$, TiO_2–B, and anatase TiO_2/TiO_2–B nanowire arrays. The spectra of $H_2Ti_2O_5$ and $H_2Ti_8O_{17}$ have peaks in the range of 2500–3500 cm^{-1}, which are due to the vibration of hydroxyl groups. According to the relationship between the O–H stretching frequencies and the H–O···H bond distances, the different peaks observed for $H_2Ti_2O_5$ (2986 cm^{-1}, 3153 cm^{-1}, and 3425 cm^{-1}) and $H_2Ti_8O_{17}$ (3161 cm^{-1}) suggest that the local structures around the H atoms in these two materials differed from each other as expected, whereas the peaks at 1405 and 1630 cm^{-1} in these two materials are ascribed to the vibration of hydroxyl groups. For the TiO_2–B and anatase TiO_2/TiO_2–B nanowires there are no absorption peaks in the range of 2500–3500 cm^{-1}, indicating that the TiO_2 phase samples do not contain H atoms in their structures.

There are two types of dehydration that can occur in $H_2Ti_2O_5 \cdot H_2O$ materials, specifically: (i) dehydration of intralayered OH groups, provided in reaction 1, or (ii) dehydration of the interlayered OH group, provided in reactions 2 and 3.[40,42]

$$H_2Ti_2O_5 \cdot H_2O \rightarrow H_2Ti_2O_5 + H_2O \quad (1)$$

$$4H_2Ti_2O_5 \rightarrow H_2Ti_8O_{17} + 3H_2O \quad (2)$$

$$H_2Ti_8O_{17} \rightarrow H_2O + 8TiO_2 \quad \text{(bronze or anatase)} \quad (3)$$

The occurrence of these two dehydration reactions can be verified by TGA data, whereby the thermogravimetric curve of the as-prepared $H_2Ti_2O_5 \cdot H_2O$ sample in the temperature range from 25 to 600 °C is provided in Figure 2b. In this figure, there are three derivative thermogravimetric (DTG) broad peaks, namely: (i) a peak observed from room temperature to 75 °C (peak at 59.6 °C), representing the desorption of physically adsorbed water (free water); (ii) a peak from 75 to 150 °C (peak at 82 °C) representing the desorption of intralayered or crystal water (reaction 1); and (iii) a peak from 150 to 400 °C (peak at 316.7 °C) representing the desorption of interlayered water (reactions 2 and 3), which reveals the transition of crystal form from orthorhombic to bronze TiO_2 through a topotactic transformation. According to the TGA data and assuming that the resulting products are TiO_2, the observed 9.8% weight loss of $H_2Ti_2O_5$ (from 100 to 600 °C) is in good agreement with the theoretical weight loss of 10.1% for the full dehydration reactions 2 and 3. Furthermore, the observed weight loss value of 6.8% for $H_2Ti_8O_{17}$ (from 100 to 250 °C) is also in good agreement with the theoretical weight loss (7.3 %). Therefore, the chemical identity of the titanium based compounds in the present study can be inferred to be $H_2Ti_2O_5$, $H_2Ti_8O_{17}$, and TiO_2 (bronze and/or anatase) in a good agreement with XRD and FTIR results.

Figure 3 and Supporting Information Figure S1 show the typical SEM images of the $H_2Ti_2O_5$, $H_2Ti_8O_{17}$, TiO_2–B, and

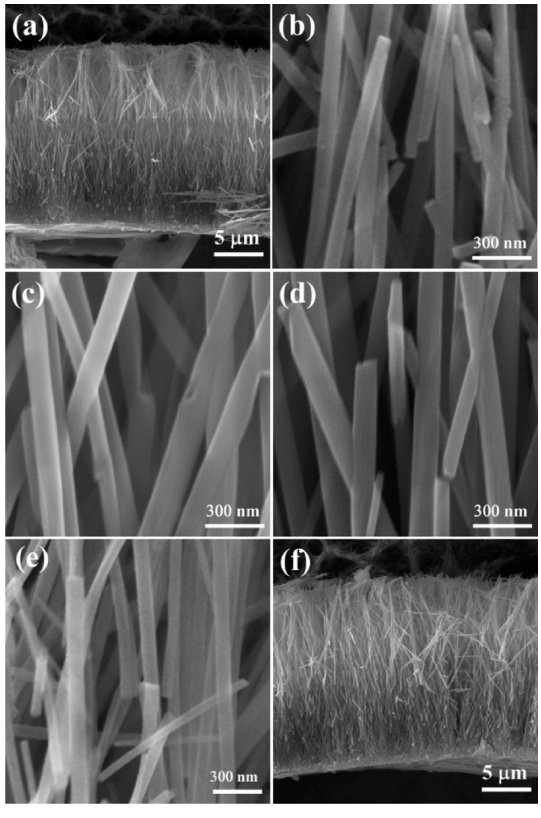

Figure 3. Cross-sectional SEM images of $H_2Ti_2O_5$ (a, b), $H_2Ti_8O_{17}$ (c), TiO_2–B (d), and anatase TiO_2/TiO_2–B (e, f).

dx.doi.org/10.1021/am4046487 | ACS Appl. Mater. Interfaces 2014, 6, 568–574

anatase TiO_2/TiO_2–B nanowire samples prepared in the present work. Figure 3a,b show the longitudinal SEM image of the $H_2Ti_2O_5$ nanowire arrays. The length and mean diameter of the $H_2Ti_2O_5$ nanowires determined from SEM imaging are around 15 μm (Figure 3a) and 80 nm (Figure 3b), respectively. When calcined from 100 to 550 °C, the bulk materials show no remarkable changes to their external morphology despite the crystal structure transformation from body-centered orthorhombic $H_2Ti_2O_5$ (Figure 3a,b) to body-centered tetragonal TiO_2;[39] however, the diameter of the nanowires undergoes a slight reduction from 80 nm for $H_2Ti_2O_5$ to about 74 nm for TiO_2 (Figure 3d,e) due to the dehydration of $H_2Ti_2O_5$ during heating.

HR-TEM images of the prepared samples annealed at different temperatures are shown in Figure 4. It is readily

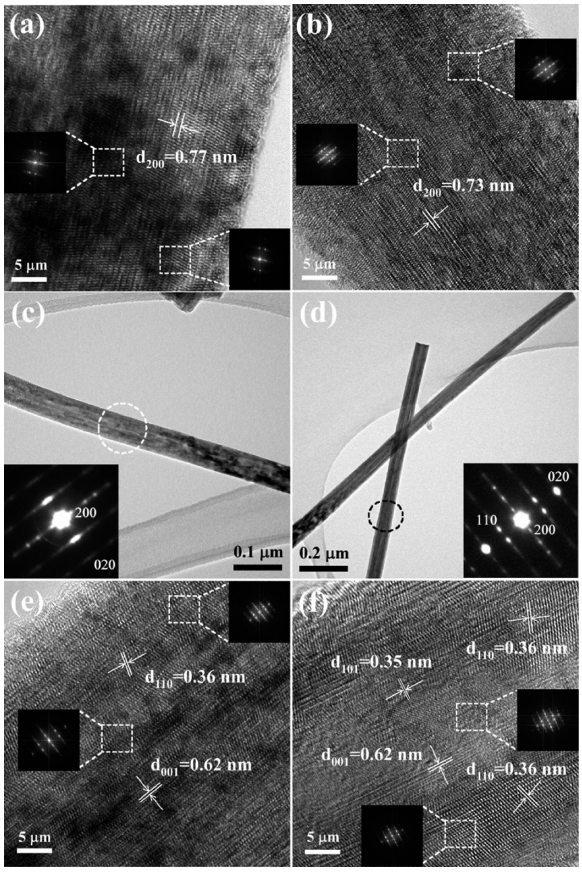

Figure 4. TEM images, FFT, and SAED patterns (inset) of $H_2Ti_2O_5$ (a), $H_2Ti_8O_{17}$ (b, c), TiO_2–B (d, e), and anatase TiO_2/TiO_2–B (f).

apparent that all prepared nanowire samples possess a single crystalline structure oriented in the [100] direction according to the SAED and FFT patterns (inset of Figure 4), which would be preferred over polycrystalline ones to obtain a faster electron transport rate. Figure 4a,b are HRTEM images of $H_2Ti_2O_5$ and $H_2Ti_8O_{17}$ annealed at 100 and 250 °C, respectively. The inter-planar spacing of d_{200} decreases from 0.80 nm for $H_2Ti_2O_5{\cdot}H_2O$ to 0.77 nm for $H_2Ti_2O_5$ and 0.73 nm for $H_2Ti_8O_{17}$, an observation that is related to the dehydration of intralayered and interlayered OH groups.[32] The inter-planar spacing could benefit the Li ion and electron transportation in batteries.[43] A detailed discussion of the formation mechanism of $H_2Ti_8O_{17}$ has been reported in previous papers.[26,42] After increasing the annealing temperature to 400 °C, a well-crystallized structure with lattice fringes of about 0.36 nm and 0.62 nm can be clearly seen in Figure 4c, which corresponds to the (110) and (001) interplanar spacings of TiO_2–B, respectively, and is consistent with previously reported values for bulk TiO_2–B phase.[44] In addition, after the annealing temperature is increased to 550 °C, the interplanar spacings of 0.35 nm, 0.36 nm, and 0.62 nm shown in Figure 4d are in excellent agreement with the *d*-spacing of the (101) plane of anatase TiO_2 and the (110) and (200) planes of TiO_2–B, respectively. Evidently, TiO_2–B is still the primarily existent crystal phase, while there is some anatase phase TiO_2 appearing in the 550 °C sample.

Figure 5 shows the cyclic voltammogram (CV) curves for $H_2Ti_2O_5$, $H_2Ti_8O_{17}$, TiO_2–B, and anatase TiO_2/TiO_2–B

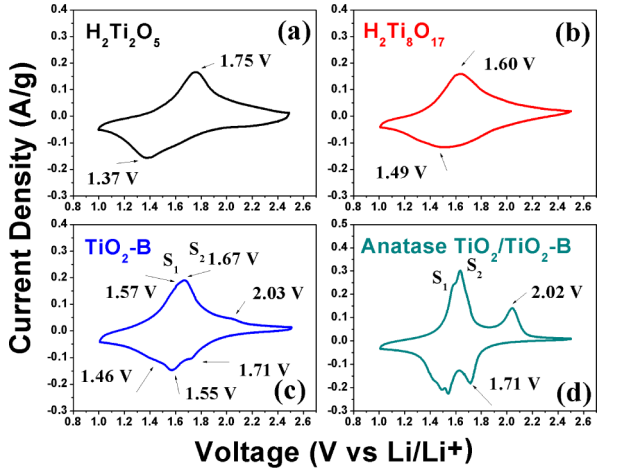

Figure 5. CV curves of $H_2Ti_2O_5$ (a), $H_2Ti_8O_{17}$ (b), TiO_2–B (c), and anatase TiO_2/TiO_2–B composite (d) electrodes at a scan rate of 0.1 mV s^{-1} between 1.0 and 2.5 V.

nanowire electrodes between 1.0 and 2.5 V (vs Li/Li^+). Only one oxidation/reduction peak is observed for the $H_2Ti_2O_5$ and $H_2Ti_8O_{17}$ electrodes, providing further indication that these materials are synthesized in pure form by the direct heat treatment process. The voltage difference between the anodic and the cathodic peak of $H_2Ti_8O_{17}$ is much lower than that of $H_2Ti_2O_5$, reflecting a weaker polarization of the electrode for the former that is consistent with the results of a previous report.[21] When the annealing temperature was set at 400 °C, two main cathodic/anodic peak pairs at 1.46 V/1.57 V (peak S1 in Figure 5c) and 1.55 V/1.67 V (peak S2 in Figure 5c) can be observed, which are attributed to the lithium ion insertion/extraction of TiO_2–B.[13] It should be noted that a third redox peak pair with a relatively small contribution was observed at 1.71 V/2.03 V, which indicates that a trace amount of anatase TiO_2 formation occurred during the annealing process which was undetected by the previously discussed characterization techniques.[9] Further increasing the annealing temperature to 550 °C, the cathodic/anodic peaks (peaks S1 and S2 in Figure 5d) of TiO_2–B became more distinct; meanwhile the intensity of the anatase TiO_2 peaks was significantly enhanced due to the transformation of TiO_2–B into anatase TiO_2.

The initial 10 charge–discharge cycle profiles for the prepared Ti-based nanowire electrodes with a current rate of 0.1 C are shown in Figure 6a–d. The initial discharge capacities were 346 mA h g^{-1} for $H_2Ti_2O_5$, 326 mA h g^{-1} for $H_2Ti_8O_{17}$, and 271 mA h g^{-1} for TiO_2–B to 247 mA h g^{-1} for anatase TiO_2/TiO_2–B electrodes. After the first cycle, the discharge

dx.doi.org/10.1021/am4046487 | ACS Appl. Mater. Interfaces 2014, 6, 568–574

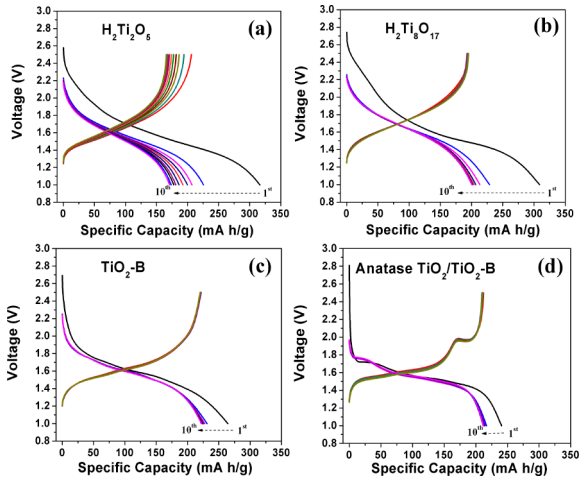

Figure 6. First 10 charge–discharge curves at 0.1 C of $H_2Ti_2O_5$ (a), $H_2Ti_8O_{17}$ (b), TiO_2–B (c), and anatase TiO_2/TiO_2–B (d) electrodes.

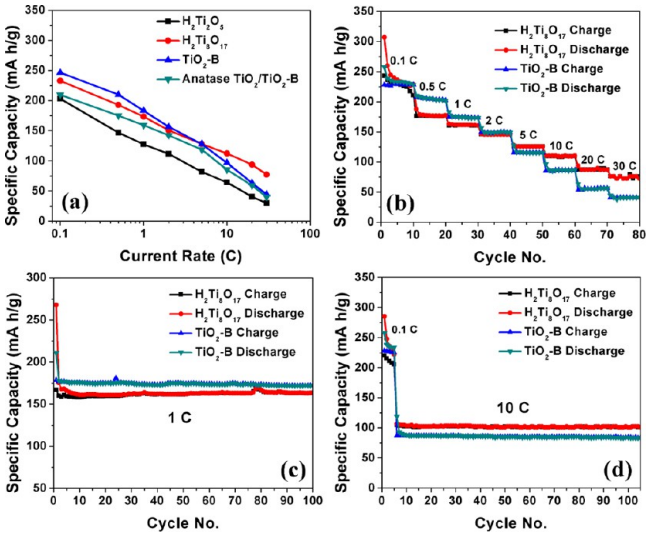

Figure 7. (a) Specific capacities of as prepared Ti-based nanowire electrodes at different current rates; (b) the discharge/charge capacities of $H_2Ti_8O_{17}$ and TiO_2–B electrodes at different current rates; (c) and (d) cyclic performance of $H_2Ti_8O_{17}$ and TiO_2–B electrodes beyond 100 cycles at a rate of 1 C and 10 C, respectively, between 1.0 and 2.5 V (vs Li/Li+). The first five cycles in (d) are conducted at a rate of 0.1 C.

capacities decreased due to the reduced number of electrons transferred per formula unit; however, the stability was gradually enhanced with an increase in annealing temperature from 100 to 550 °C. For HTO nanowire electrodes (Figure 5a,b) the average working voltage decreased from approximately 1.75 V to 1.62 V after two cycles, suggesting that the H^+/Li^+ ion-exchange reaction occurred during the initial battery cycling. This observation is consistent with a previous report on $H_2Ti_3O_7$ based electrodes, in which XRD analysis indicated the production of a layered $Li_2Ti_3O_7$ phase after cycling tests.[40] Furthermore, the large irreversible insertion capacity during the initial two cycles suggested formation of the Ti^{3+} containing compound $Li_xH_2Ti^{3+}{}_yTi^{4+}{}_zO_{5(17)}$ during the first Li insertion reaction. Figure 6c,d present the electrochemical Li insertion–extraction properties of TiO_2–B and anatase TiO_2/TiO_2–B nanowires, respectively. Particularly, TiO_2–B shows a working potential of around 1.6 V, whereas the anatase TiO_2/TiO_2–B composite electrode depicts two voltage plateaus on both the discharge and charge curves. This is in agreement with the cathodic/anodic peak potentials observed in the CV curves and attributed to the presence of both the TiO_2–B and anatase TiO_2 phases. It is worth noting that a stable reversible capacity of approximately of 225 mA h g^{-1} for TiO_2–B and 215 mA h g^{-1} for anatase TiO_2/TiO_2–B composite electrodes were observed during the 2nd through 10th cycles.

Figure 7a show the variations in the cell capacity as a function of the applied current rate, expressed in terms of C (1 C = 335 mA g^{-1}). $H_2Ti_8O_{17}$ and TiO_2–B nanowire electrodes exhibit higher rate capability compared with the other two electrodes. Closer comparison between these two electrodes at various charge–discharge rates from 0.1 C to 30 C are shown in Figure 7b. The $H_2Ti_8O_{17}$ nanowire arrays show a lower rate performance at low current rates from 0.1 C to 2 C but superior rate capabilities at higher rates from 5 C to 30 C. Specifically, the $H_2Ti_8O_{17}$ electrode has a superior rate performance with discharge capacities of 127.2, 111.4, 87.2, and 73.5 mA h g^{-1} at 5 C, 10 C, 20 C, and 30 C, respectively, while the TiO_2–B electrode has discharge capacities of only 115.6, 87.2, 56.8, and 41.0 mA h g^{-1} at 5 C, 10 C, 20 C, and 30 C, respectively. Figure 7c compares the cycling performance of these two electrodes at a rate of 1 C (lower current rate). As shown in Figure 7c, the TiO_2–B nanowire electrode demonstrates a slightly higher capacity than that of $H_2Ti_8O_{17}$; however, both of them indicated excellent durability after 10 cycles. Specifically, the discharge capacities of $H_2Ti_8O_{17}$ and TiO_2–B nanowire electrodes were maintained at 163.7 mA h g^{-1} and 172.1 mA h g^{-1} after 100 cycles, respectively. After 500 cycles, in the case of $H_2Ti_8O_{17}$, the discharge capacity was measured to be 157.8 mA h g^{-1} (96.4% of 100th discharge capacity) with a coulombic efficiency of 100% (Supporting Information Figure S2). The cycling performance at a high current rate of 10 C after 5 cycles at a rate of 0.21 C in the same voltage range for the two electrodes are shown in Figure 7d. The $H_2Ti_8O_{17}$ electrode shows a higher capacity and better cycling performance. There is minimal capacity fading even after 100 cycles for the $H_2Ti_8O_{17}$ nanowire electrode, corresponding to only a 4.7% loss compared to 13% for the TiO_2–B nanowire electrode. On the basis of this minimal loss observed after 100 cycles, it can be expected that no significant morphological changes or crystallite degradation occurred during charge/discharge for $H_2Ti_8O_{17}$ nanowire electrode.[24] The greatly improved lithium storage properties including capacity, rate capability, and cycling performance of single crystalline $H_2Ti_8O_{17}$ nanowire array electrodes in comparison to TiO_2–B could be attributed to its high electronic conductivity. Moreover, when measured at 10 C up to 100 cycles, the discharge capacity of the $H_2Ti_8O_{17}$ electrode depicted a higher capacity along with excellent capacity retention (118 mA h g^{-1} or 93% of the initial discharge capacity).

Electrochemical impedance spectroscopy (EIS) measurements were carried out in order to compare the conductivity of the prepared $H_2Ti_8O_{17}$ and TiO_2–B nanowire electrodes. The corresponding Nyquist plots after cycling five times at a rate of 0.1 C, as well as the fitting results using an equivalent circuit of both electrodes, are shown in Figure 8. In the equivalent circuit (Figure 8 inset), R_s and R_{ct} are the ohmic resistance (total resistance of the electrolyte, separator, and electrical contacts) and charge transfer resistance, respectively. W represents the Warburg impedance of Li ion diffusion into the active materials.

dx.doi.org/10.1021/am4046487 | ACS Appl. Mater. Interfaces 2014, 6, 568–574

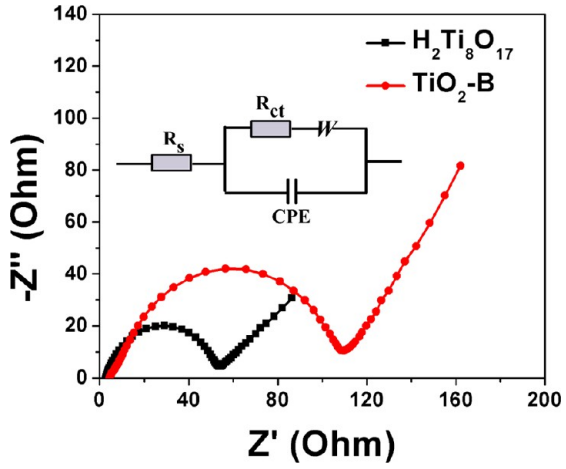

Figure 8. Electrochemical impedance spectra (Nyquist plots) of $H_2Ti_8O_{17}$ and TiO_2–B electrodes after cycling five times at 0.1 C.

CPE is the constant phase-angle element, involving double layer capacitance. The system resistance of R_s is similar for $H_2Ti_8O_{17}$ and TiO_2–B electrodes. This is due to the fact that both materials are grown directly on the substrates that are used at the current collectors, which ensures good electrical conductivity in the electrodes. The $H_2Ti_8O_{17}$ nanowire electrode exhibits lower charge transfer resistance (51.4 ohm) than that of TiO_2–B electrode (109.2 ohm), indicating that the single crystalline $H_2Ti_8O_{17}$ nanowires prepared at 250 °C could enable much easier charge transfer at the electrode/electrolyte interface and faster electron transportation due to the larger interlayer spacing compared to that of TiO_2–B (Figure 4b,e), and consequently will decrease the overall resistance. Higher inter-planar spacings could provide beneficial enhancements to the Li ion and electron transport through the battery electrodes, providing reasonable evidence for the decreased charge transfer resistance of $H_2Ti_8O_{17}$.[43] The lower charge transfer resistance (R_{ct}) can provide logical explanation for the increased rate performance for $H_2Ti_8O_{17}$ in comparison with TiO_2–B at higher current rates from 5 C to 30 C (Figure 7 b,d).

4. CONCLUSIONS

In summary, crystalline self-supported, 3D single crystalline nanowire array electrodes were prepared by innovatively coupling a simplistic hydrothermal procedure to fabricate $H_2Ti_2O_5{\cdot}H_2O$ nanowires, with a heat treatment in air. Using varying temperatures, $H_2Ti_2O_5$, $H_2Ti_8O_{17}$, TiO_2–B, and anatase TiO_2/TiO_2–B phase nanowire arrays supported directly on current collectors were successfully prepared for the first time, and their electrochemical characteristics were investigated towards LIBs. The electrochemical results clearly demonstrated that the single crystalline $H_2Ti_8O_{17}$ nanowire array electrode exhibited good cycling performance with a discharge capacity greater than 160 mA h g^{-1} and a capacity retention rate of 96.3% even after 500 cycles at a current rate of 1 C. Moreover, when measured at a high current rate of 10 C, up to 100 cycles, the discharge capacity of the $H_2Ti_8O_{17}$ electrode depicted a higher capacity and stability (101 mA h g^{-1} and 95.3% of initial discharge capacity retention) compared to the other three nanowire array electrodes. Accordingly, the prepared self-supported single crystalline $H_2Ti_8O_{17}$ nanowire arrays are presented as very promising high rate oxide anode materials for advanced lithium ion battery applications.

ASSOCIATED CONTENT

Supporting Information

Top-view SEM image of $H_2Ti_8O_{17}$ nanowire arrays and cycle performance of $H_2Ti_8O_{17}$ electrode beyond 500 cycles at a rate of 1 C. This material is available free of charge via the Internet at http://pubs.acs.org.

AUTHOR INFORMATION

Corresponding Authors

*X.X. E-mail: xingcheng.xiao@gm.com.
*Z.C. E-mail: zhwchen@uwaterloo.ca.

Notes

The authors declare no competing financial interest.

ACKNOWLEDGMENTS

This work was financially supported by the Natural Sciences and Engineering Research Council of Canada (NSERC), the University of Waterloo, and the Waterloo Institute for Nanotechnology. The authors thank Mr. Hey Woong Park, Mr. Victor Chabot, Mr. Drew Higgins, and Mr. Gregory Lui at the University of Waterloo for their help in editing the manuscript.

REFERENCES

(1) Ji, L. W.; Lin, Z.; Alcoutlabi, M.; Zhang, X. W. *Energy Environ. Sci.* **2011**, *4*, 2682–2699.
(2) Bruce, P. G.; Scrosati, B.; Tarascon, J. M. *Angew. Chem., Int. Ed.* **2008**, *47*, 2930–2946.
(3) Zheng, G. Y.; Yang, Y.; Cha, J. J.; Hong, S. S.; Cui, Y. *Nano Lett.* **2011**, *11*, 4462–4467.
(4) Li, X. F.; Meng, X. B.; Liu, J.; Geng, D. S.; Zhang, Y.; Banis, M. N.; Li, Y. L.; Yang, J. L.; Li, R. Y.; Sun, X. L.; Cai, M.; Verbrugge, M. W. *Adv. Funct. Mater.* **2012**, *22*, 1647–1654.
(5) Wang, J. J.; Sun, X. L. *Energy Environ. Sci.* **2012**, *5*, 5163–5185.
(6) Jung, Y. S.; Cavanagh, A. S.; Gedvilas, L.; Widjonarko, N. E.; Scott, I. D.; Lee, S. H.; Kim, G. H.; George, S. M.; Dillon, A. C. *Adv. Energy Mater.* **2012**, *2*, 1022–1027.
(7) Wang, F.; Robert, R.; Chernova, N. A.; Pereira, N.; Omenya, F.; Badway, F.; Hua, X.; Ruotolo, M.; Zhang, R. G.; Wu, L. J.; Volkov, V.; Su, D.; Key, B.; Whittingharn, M. S.; Grey, C. P.; Amatucci, G. G.; Zhu, Y. M.; Graetz, J. *J. Am. Chem. Soc.* **2011**, *133*, 18828–18836.
(8) Zhu, G. N.; Wang, Y. G.; Xia, Y. Y. *Energy Environ. Sci.* **2012**, *5*, 6652–6667.
(9) Cui, L. F.; Yang, Y.; Hsu, C. M.; Cui, Y. *Nano Lett.* **2009**, *9*, 3370–3374.
(10) Wang, J.; Verbrugge, M. W.; Liu, P. *J. Electrochem. Soc.* **2010**, *157*, A185–A189.
(11) Mukhopadhyay, A.; Tokranov, A.; Xiao, X. C.; Sheldon, B. W. *Electrochim. Acta* **2012**, *66*, 28–37.
(12) Wang, Y.-Q.; Gu, L.; Guo, Y.-G.; Li, H.; He, X.-Q.; Tsukimoto, S.; Ikuhara, Y.; Wan, L.-J. *J. Am. Chem. Soc.* **2012**, *134*, 7874–7879.
(13) Liu, H. S.; Bi, Z. H.; Sun, X. G.; Unocic, R. R.; Paranthaman, M. P.; Dai, S.; Brown, G. M. *Adv. Mater.* **2011**, *23*, 3450–3457.
(14) Chen, Z. H.; Qin, Y.; Ren, Y.; Lu, W. Q.; Orendorff, C.; Roth, E. P.; Amine, K. *Energy Environ. Sci.* **2011**, *4*, 4023–4030.
(15) Yu, A. P.; Park, H. W.; Davies, A.; Higgins, D. C.; Chen, Z. W.; Xiao, X. C. *J. Phys. Chem. Lett.* **2011**, *2*, 1855–1860.
(16) Yang, Z. X.; Du, G. D.; Guo, Z. P.; Yu, X. B.; Chen, Z. X.; Guo, T. L.; Liu, H. K. *J. Mater. Chem.* **2011**, *21*, 8591–8596.
(17) Liu, B.; Deng, D.; Lee, J. Y.; Aydil, E. S. *J. Mater. Res.* **2010**, *25*, 1588–1594.
(18) Zhao, L.; Hu, Y. S.; Li, H.; Wang, Z. X.; Chen, L. Q. *Adv. Mater.* **2011**, *23*, 1385–1388.

(19) Wang, H. E.; Lu, Z. G.; Xi, L. J.; Ma, R. G.; Wang, C. D.; Zapien, J. A.; Bello, I. *ACS Appl. Mater. Interfaces* **2012**, *4*, 1608−1613.
(20) Ren, Y. M.; Zhang, J.; Liu, Y. Y.; Li, H. B.; Wei, H. J.; Li, B. J.; Wang, X. Y. *ACS Appl. Mater. Interfaces* **2012**, *4*, 4776−4780.
(21) Rahman, M. M.; Wang, J. Z.; Hassan, M. F.; Wexler, D.; Liu, H. K. *Adv. Energy Mater.* **2011**, *1*, 212−220.
(22) Liao, J. Y.; Xiao, X. C.; Higgins, D.; Lee, D. U.; Hassan, F.; Chen, Z. W. *Electrochim. Acta* **2013**, *108*, 4−11.
(23) Liu, S. H.; Jia, H. P.; Han, L.; Wang, J. L.; Gao, P. F.; Xu, D. D.; Yang, J.; Che, S. N. *Adv. Mater.* **2012**, *24*, 3201−3204.
(24) Akimoto, J.; Chiba, K.; Kijima, N.; Hayakawa, H.; Hayashi, S.; Gotoh, Y.; Idemoto, Y. *J. Electrochem. Soc.* **2011**, *158*, A546−A549.
(25) Zhang, H.; Li, G. R.; An, L. P.; Yan, T. Y.; Gao, X. P.; Zhu, H. Y. *J. Phys. Chem. C* **2007**, *111*, 6143−6148.
(26) Suzuki, S.; Miyayama, M. *J. Ceram. Soc. Jpn.* **2010**, *118*, 1154−1158.
(27) Liu, H.; Fu, L. J.; Zhang, H. P.; Gao, J.; Li, C.; Wu, Y. P.; Wu, H. Q. *Electrochem. Solid State Lett.* **2006**, *9*, A529−A533.
(28) Ali, Z.; Cha, S. N.; Sohn, J. I.; Shakir, I.; Yan, C.; Kim, J. M.; Kang, D. J. *J. Mater. Chem.* **2012**, *22*, 17625−17629.
(29) Liu, Y. H.; Zhang, W.; Zhu, Y. J.; Luo, Y. T.; Xu, Y. H.; Brown, A.; Culver, J. N.; Lundgren, C. A.; Xu, K.; Wang, Y.; Wang, C. S. *Nano Lett.* **2013**, *13*, 293−300.
(30) Shaijumon, M. M.; Perre, E.; Daffos, B.; Taberna, P. L.; Tarascon, J. M.; Simon, P. *Adv. Mater.* **2010**, *22*, 4978−4981.
(31) Liao, J. Y.; Higgins, D.; Lui, G.; Chabot, V.; Xiao, X. C.; Chen, Z. W. *Nano Lett.* **2013**, *11*, 5467−5473.
(32) Shen, L. F.; Uchaker, E.; Zhang, X. G.; Cao, G. Z. *Adv. Mater.* **2012**, *24*, 6502−6506.
(33) Li, Y. G.; Tan, B.; Wu, Y. Y. *Nano Lett.* **2008**, *8*, 265−270.
(34) Ko, Y. D.; Kang, J. G.; Park, J. G.; Lee, S.; Kim, D. W. *Nanotechnology* **2009**, *20*, 455701.
(35) Wang, L. L.; Wu, X. M.; Zhang, S. C. *Mech. Electron. Eng. III, Pts. 1−5* **2012**, *130-134*, 1281−1285.
(36) Renner, F. U.; Kageyama, H.; Siroma, Z.; Shikano, M.; Schoder, S.; Grunder, Y.; Sakata, O. *Electrochim. Acta* **2008**, *53*, 6064−6069.
(37) Foll, H.; Carstensen, J.; Ossei-Wusu, E.; Cojocaru, A.; Quiroga-Gonzalez, E.; Neumann, G. *J. Electrochem. Soc.* **2011**, *158*, A580−A584.
(38) Liu, B.; Aydil, E. S. *J. Am. Chem. Soc.* **2009**, *131*, 3985−3990.
(39) Liu, B.; Boercker, J. E.; Aydil, E. S. *Nanotechnology* **2008**, *19*, 505604.
(40) Liao, J. Y.; Lei, B. X.; Chen, H. Y.; Kuang, D. B.; Su, C. Y. *Energy Environ. Sci.* **2012**, *5*, 5750−5757.
(41) Izawa, H.; Kikkawa, S.; Koizumi, M. *J. Phys. Chem* **1982**, *86*, 5023−5026.
(42) Zhang, M.; Jin, Z. S.; Zhang, J. W.; Guo, X. Y.; Yang, H. J.; Li, W.; Wang, X. D.; Zhang, Z. J. *J. Mol. Catal. A: Chem.* **2004**, *217*, 203−210.
(43) Wei, M.; Wei, K.; Ichiharac, M.; Zhou, H. *Electrochem. Commun.* **2008**, *10*, 1164−1167.
(44) Zukalova, M.; Kalbac, M.; Kavan, L.; Exnar, I.; Graetzel, M. *Chem. Mater.* **2005**, *17*, 1248−1255.